sciendo | Journal of Electrical Bioimpedance | JoEB bioimpedance.net

J Electr Bioimp, vol. 14, pp. 19-31, 2023
Received 4 Jul 2023 / published 5 Aug 2023
https://doi.org/10.2478/joeb-2023-0004

Skin layer classification by feedforward neural network in bioelectrical impedance spectroscopy

Kiagus Aufa Ibrahim [1], Marlin Ramadhan Baidillah [2,4], Ridwan Wicaksono [3], and Masahiro Takei [1]

1. *Department of Mechanical Engineering, Graduate School of Science and Engineering, Chiba University, Chiba, Japan*
2. *Research Center for Electronics, National Research and Innovation Agency, KST Samaun Samadikun, Bandung, Indonesia*
3. *Electrical and Information Engineering Department, Faculty of Engineering, Universitas Gadjah Mada, Yogyakarta, Indonesia*
4. *E-mail any correspondence to: marlin.ramadhan.baidillah@brin.go.id*

Abstract

Conductivity change in skin layers has been classified by source indicator o^k (k=1: Stratum corneum, k=2: Epidermis, k=3: Dermis, k=4: Fat, and k=5: Stratum corneum + Epidermis) trained from feedforward neural network (FNN) in bioelectrical impedance spectroscopy (BIS). In BIS studies, treating the skin as a bulk, limits the differentiation of conductivity changes in individual skin layers, however skin layer classification using FNN shows promise in accurately categorizing skin layers, which is essential for predicting source indicators o^k and initiating skin dielectric characteristics diagnosis. The o^k is trained by three main conceptual points which are (i) implementing FNN for predicting k in conductivity change, (ii) profiling four impedance inputs α_ξ consisting of magnitude input $\alpha_{|Z|}$, phase angle input α_θ, resistance input α_R, and reactance input α_X for filtering nonessential input, and (iii) selecting low and high frequency pair (f_r^{lh}) by distribution of relaxation time (DRT) for eliminating parasitic noise effect. The training data set of FNN is generated to obtain the $\alpha_\xi \in \boldsymbol{R}^{10\times17\times10}$ by 10,200 cases by simulation under configuration and measurement parameters. The trained skin layer classification is validated through experiments with porcine skin under various sodium chloride (NaCl) solutions $c_{NaCl} = \{15, 20, 25, 30, 35\}[\mathrm{mM}]$ in the dermis layer. FNN successfully classified conductivity change in the dermis layer from experiment with accuracy of 90.6% for the bipolar set-up at $f_6^{lh} = 10\ \&\ 100\ [\mathrm{kHz}]$ and with the same accuracy for the tetrapolar at $f_8^{lh} = 35\ \&\ 100\ [\mathrm{kHz}]$. The measurement noise and systematic error in the experimental results are minimized by the proposed method using the feature extraction based on α_ξ at f_r^{lh}.

Keywords: Bioelectrical impedance spectroscopy; Conductivity change; Distribution of relaxation times; Feedforward neural network

Introduction

Skin is a multi-layer dielectric medium with different electrical properties related to structural characteristics [1], chemical composition variations [2], and different biological functions, in which the assessment of each layer leads to a better understanding of its pathophysiology. As a common modality to measure dielectric characteristics in biological tissue, bioelectrical impedance spectroscopy (BIS) is well-known as low-cost, sensitive to chemical composition, and portable for clinical measurement, which is capable of measuring the electrical conductivity of the human skin layer [3]. BIS for human skin is utilized to assess skin rubor (or erythema) [4], skin cancer [5], diabetes [6], edema [7], skin irritation [8], skin thickness [9], and drug delivery [10]. Each skin layer contributes differently, allowing current to flow during measurement. Thus, any conductivity change in each skin layer affects the measured impedance. However, most BIS studies considered skin as a bulk instead of having layer composition. In the case of the conductivity change occuring at a particular skin layer, the traditional BIS shows the impedance change but cannot determine which skin layer has changed its conductivity because the equivalent circuits of each layer are connected and behave as a parallel circuit.

© 2023 Author(s). This is an open access article licensed under the Creative Commons Attribution License 4.0. (http://creativecommons.org/licenses/by/4.0/).

Consequently, BIS is not able to solve the indistinguishability of skin layers in conductivity change.

In order to solve the problem, skin layer classification by machine learning algorithm (MLA) is introduced. MLA have been proposed by some studies such as Natasha et al. to detect breast cancer [11], Gessert et al. to detect melanoma [12], and Kawahara et al. to detect skin lesions [13]. The studies of tissue disorders based on BIS and MLA illustrate the ability of MLA skin layer classification. For impedance measurements, Feedforward Neural Network (FNN) is appropriate because it can model complex relationships between inputs and outputs, making it a powerful tool for high-accuracy classification tasks that can be performed quickly with less computational power and can use parallel computation to increase the algorithm's efficiency [14]. The skin layer classification based on impedance measurement, which focuses specifically on predicting source indicator o^k, is a preliminary step to skin dielectric characteristics diagnosis. FNN is employed for predicting source indicator o^k.

As a post-processing BIS for predicting conductivity change in time domain, the distribution of relaxation times (DRT) [15] was proposed. By the principle of superposition, the impedance can be represented as a series connection of an infinite number of electrical equivalent circuit (EEC) made of a parallel connection of a resistive polarization part and a capacitive part [16]. DRT assumes that the measured impedance is an infinite number of RC elements with continuous relaxation time [17]. However, DRT requires knowledge of baseline value of the conductivity change on a specific time constant. Any conductivity changes with frequency-dependent behaviour affect the amplitude of the relaxation time function, which is not limited to one time constant. Thus, DRT is adequately used whenever the unwanted conductivity change can be detected and eliminated. The baseline value with a known conductivity value prior to the impedance measurement is needed to classify the skin conditions in the time domain, which is related to a conductivity change in a specific skin layer. Otherwise, the conductivity change cannot be classified. To overcome this challenge, four impedance inputs α_ξ with time-difference analysis are introduced.

In order to overcome the baseline value problem and to determine the desired skin layer accurately, the impedance changes of BIS are transformed into four impedance inputs α_ξ of FNN. They are presented with time-difference analysis, which are the magnitude input (MX) $\alpha_{|Z|}$, phase angle input (PX) α_θ, resistance input (RX) α_R, and reactance input (IX) α_X. The MX, PX, RX and IX have been proposed by Ollmar et al. without considering the time difference analysis in order to diagnose the oral mucosa which are chosen solely based on physically fundamental aspects of the behavior of skin in the lower frequency and higher frequency [18]. Additionally, to increase the relation of training data features with the FNN results, two possible injection patterns φ_s, which are Bipolar and Tetrapolar, are presented and compared with each other. The two injection patterns φ_s have different performances in extracting the electrical properties of the viable tissues because the electrode-length-to-skin-thickness ratio δ_b significantly affects the electrical current penetration depth.

Conductivity change related to physiological change is always affected by parasitic noise, such as variation of temperature or moisture content in the tissues. Hence, the parasitic noise effect on impedance measurements can be eliminated by selecting the frequency pair whose effect is negligible. In this regard, DRT is employed to select the frequency pair where the conductivity changes from the skin layer more dominantly than other conductivity sources.

Therefore, we come up with three main conceptual points, which are (i) FNN implementation for predicting o^k in conductivity change, (ii) four impedance inputs α_ξ profiles consisting of magnitude input $\alpha_{|Z|}$, phase angle input α_θ, resistance input α_R, and reactance input α_X, and (iii) frequency pair f_r^{lh} selection by the distribution of relaxation time (DRT) in order to accurately predict the conductivity change in the skin layer. In summary, Appendix A shows the comparison with the related literature studies to highlight the contribution of this study.

This paper presents a skin layer classification method employing FNN based on the conductivity change measured by bioelectrical impedance spectroscopy. In this study, three objectives are presented, which are (1) The validation accuracy of source indicator o^k trained from FNN, (2) The validation accuracy based on experiment, and (3) Impedance inputs α_ξ evaluation in performing feature extraction.

Skin layers classification of conductivity change in skin layers by source indicator trained from FNN

Implementing FNN for predicting k *in conductivity change*

Fig. 1 shows the schematic flow of FNN. FNN is a fully connected layer of the neural network and connections from the network inputs to each subsequent layer from the previous layer, known as multi-layer perceptron (MLP). A structure of FNN consists of one hidden layer with 100 neurons, the four impedance inputs α_ξ in the input layer, and the five source indicators o^k in the output layer. This fully connected FNN structure has $(\xi \times u) + (u \times o)$ total number of weight connections, where $\xi = \{1, \dots, \Xi\}$ is data input in the input layer, $u = \{1, \dots, U\}$ is neuron in the hidden layer, and $o = \{1, \dots, O\}$ is the number of data output in the output layer. The weight connections are used in order to perform the computation. The computation steps of the network of one hidden layer for *n*th sample in training data set is as follows:

1) The first step is summing the weights in the hidden layer:

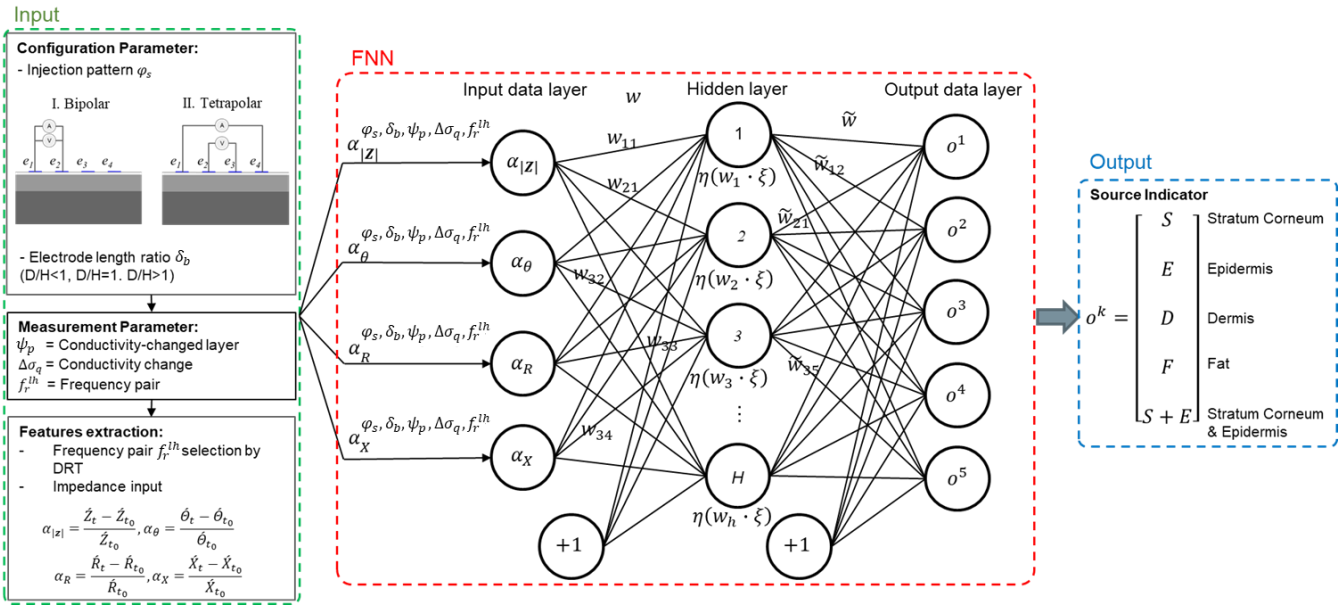


Fig.1: Schematic flow of skin layer classification of conductivity change

$$S_u^n = \sum_1^U w_{u\xi}\,\alpha_\xi + \beta_\xi \tag{1}$$

where α_ξ is the input data (which are impedance inputs), $w_{u\xi}$ is the weight vector connecting the input neurons ξth and the hidden layer neuron uth, and β_ξ is the input variable's bias term,

2) The second step is feeding the summations of the first step NN computation to the neurons' output using the rectified linear unit (ReLU) activation function g_u:

$$g_u(S_u^n) = \begin{cases} S_u^n, & S_u^n > 0 \\ 0, & S_u^n \le 0 \end{cases} \tag{2}$$

where S_u^n is the sum of weights,

3) The last step is calculating the output neurons:

$$y_o^n = \sum_1^U \widetilde{w}_{uo}\,g_u + \beta_u \tag{3}$$

where y_u^n is the output of hidden layer neuron uth, $\widetilde{w}_{uo}$ is the weight between the output variable y_o^n and hidden layer neuron uth, β_u is the output variable's bias term, n is the number of samples which is F (number of frequency pair of lower frequency and higher frequency) times t (number of impedance measurements in a time domain), $F = \{1, \dots, \Gamma\}$, and $t = \{1, \dots, T\}$.

The training process based on the supervised learning employs a tuning process to control the weight ($w_{u\xi}$ and $\widetilde{w}_{uo}$) and bias (β_ξ and β_u) parameters based on the minimizing of error rate including both skin layer classification and approximation errors.

Profiling four impedance inputs α_ξ

In order to minimize the unnecessary training data of FNN, this study introduces impedance inputs α_ξ as a data feature extraction which are the magnitude input (MX) $\alpha_{|Z|}$, phase angle input (PX) α_θ, resistance input (RX) α_R, and reactance input (IX) α_X. Considering that the skin layer classification of conductivity change is in the time domain. Thus, the impedance inputs α_ξ in the time domain are as the following equations:

$$\alpha_{|Z|} = \frac{\acute{Z}_t - \acute{Z}_{t_0}}{\acute{Z}_{t_0}} \tag{4}$$

$$\alpha_\theta = \frac{\acute{\theta}_t - \acute{\theta}_{t_0}}{\acute{\theta}_{t_0}} \tag{5}$$

$$\alpha_R = \frac{\acute{R}_t - \acute{R}_{t_0}}{\acute{R}_{t_0}} \tag{6}$$

$$\alpha_X = \frac{\acute{X}_t - \acute{X}_{t_0}}{\acute{X}_{t_0}} \tag{7}$$

where,

$$\acute{Z} = \frac{\mathrm{abs}(Z_l)}{\mathrm{abs}(Z_h)} \tag{8}$$

$$\acute{\theta} = \arg(Z_l) - \arg(Z_h) \tag{9}$$

$$\acute{R} = \frac{\mathrm{re}(Z_l)}{\mathrm{abs}(Z_h)} \tag{10}$$

$$\acute{X} = \frac{\mathrm{im}(Z_l)}{\mathrm{abs}(Z_h)} \tag{11}$$

where t is an arbitrary amount of time after a reference time t_0, $abs(Z)$ is the magnitude (modulus) of the complex

electrical impedance, $arg(Z)$ is the argument (phase angle) in degrees, $re(Z)$ is the resistance of the complex electrical impedance ($re(Z) = abs(Z) * cos\ [arg(Z)]$), and $im(Z)$ is the reactance of the complex electrical impedance ($im(Z) = abs(Z) * sin\ [arg(Z)]$). Z_l and Z_h represent the impedance at low and high frequencies, respectively, where the frequencies are based on the frequency pair f_r^{lh} selection.

In fact, any change in conductivity σ and permittivity ε_r of the skin layer affects all α_ξ. The $\acute{R}$ reflects conductivity changes; the $\acute{X}$ reflects mainly reactance changes, which are of capacitive nature; the $\acute{Z}$ reflects changes along the length of the vector describing the impedance in complex space, which is emphasized if the real and reactance change are in the same direction and proportion; the $\acute{\theta}$ is emphasized if the real and reactance change are in different directions and different proportions. All α_ξ reside solely on physically fundamental aspects of the behavior of electrical impedance in the selected frequency range [7]. Thus, the accuracy of equations (4) to (7) depends on the frequency pair f_r^{lh} selection. The DRT is used to select the frequency pair based on the time-constant domain, which is related with the skin layer as explained in the next subsection.

Selecting frequency pair f_r^{lh} by distribution of relaxation times (DRT)

The predicted impedance of DRT Z_{drt} [Ω] is represented by the following equation:

$$Z_{drt}(f) = R_\infty + \int_0^\infty \frac{\gamma(\ln\tau)}{1 + j2\pi f\tau}\mathrm{d}(\ln\tau) \qquad (12)$$

where R_∞ [Ω] is resistance at the high frequency, $\gamma(\ln\tau)$[Ω] is the distribution function of the total polarization resistance along the relaxation time τ[s], and $\int_{-\infty}^{\infty}\gamma(\ln\tau)\mathrm{d}(\ln\tau) = R_p$ is a normalized function over the entire relaxation time τ where R_p is the polarization resistance.

In order to retrieve the distribution of $\gamma(\ln\tau)$, an approximation by the sum of *M* radial basis function (RBFs) is used. Hence, equation (12) can be expressed as follows [17]:

$$Z_{\mathrm{drt}}(f;\boldsymbol{\Theta}) = R_\infty + \sum_{m=1}^{M}\Theta_m\int_0^\infty \frac{g_m(\ln\tau)}{1 + j2\pi f\tau}\mathrm{d}(\ln\tau) \qquad (13)$$

where, $g_m(\ln\tau) \triangleq e^{-(\mu(|\ln\tau - \ln\tau_m|))^2}$ [Ω] is the RBFs with each function is center at the relaxation time τ_m and a full width at half maximum (FWHM) as μ. While $\boldsymbol{\Theta} = [\Theta_1, \cdots, \Theta_M]^T$ is a vector parameter related to the amplitude of RBFs.

Calculating the $\gamma(\ln\tau)$ in equation (13) is an ill-posed problem case. Currently, there are several available methods to overcome the DRT ill-posed problem: an evolutionary programming method proposed by Oz et al. [19], a monte-carlo method proposed by Tuncer and McDonald [20], a discrete Fourier transformation proposed by Schichlein et al. [21] and a fitting approach proposed by Sonn et al. [22]. Using a discrete Fourier transformation is not trivial because of requiring an indispensable data exploration and filtering of high-quality impedance data [23]. Alternatively, a fitting approach for DRT is proposed based on fitting the resistance of the spectra to a number of RC elements with fixed time constants [22]. A further improvement by the Ciucci research group for the fitting approach is employing a Tikhonov regularization [16]. In this study, a mathematical toolbox called the DRTtools toolbox proposed by Wan et al. is used. The main goal is to fit the data between the impedance Z_{exp} [Ω] from experiment against with the model Z_{drt} by optimization of $\gamma(\ln\tau)$ [16]. The optimization of $\gamma(\ln\tau)$ is retrieved as the optimal parameters vector $\boldsymbol{\Theta}^* = \underset{\Theta:\Theta\geq 0}{\mathrm{argmin}}\,\boldsymbol{V}(\boldsymbol{\Theta})$ by minimizing the error least square between the measured impedance and the predicted impedance as follows:

$$\boldsymbol{V}(\boldsymbol{\Theta}) = \left\|\left(\left(R_\infty\mathbf{1}\right) + \boldsymbol{A}^{\mathrm{re}}\boldsymbol{\Theta}\right) - \boldsymbol{Z}_{\mathrm{exp}}^{\mathrm{re}}\right\|_2^2 + \left\|\left(\boldsymbol{A}^{\mathrm{im}}\boldsymbol{\Theta}\right) - \boldsymbol{Z}_{\mathrm{exp}}^{\mathrm{im}}\right\|_2^2 + \lambda\|\boldsymbol{\Theta}\|_2^2 \qquad (14)$$

where L is the number of frequency points, $\lambda > 0$ is the hyperparameters to tune the error computation, and $\mathbf{A}^{\mathrm{re}} \in \mathbb{R}^{L\times M}$ and $\mathbf{A}^{\mathrm{im}} \in \mathbb{R}^{L\times M}$ are the matrix notion of parameters obtained from the real Z_{drt}^{re} and reactance Z_{drt}^{im} of the predicted impedance Z_{drt}, which are expressed as follows:

$$Z_{drt}^{re} = R_\infty + \sum_{m=1}^{M}\Theta_m\underbrace{\left[\int_0^\infty \frac{g_m(\ln\tau)}{1 + (2\pi f\tau)^2}\mathrm{d}\,(\ln\tau)\right]}_{A^{\mathrm{re}}} \qquad (15)$$

$$Z_{drt}^{im} = -\sum_{m=1}^{M}\Theta_m\underbrace{\left[\int_0^\infty \frac{2\pi f\tau\, g_m(\ln\tau)}{1 + (2\pi f\tau)^2}\mathrm{d}\,(\ln\tau)\right]}_{A^{\mathrm{im}}} \qquad (16)$$

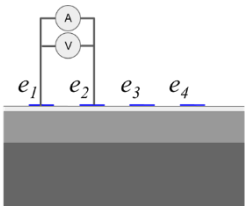
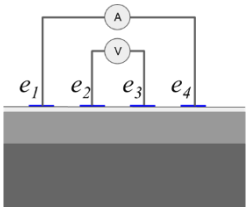
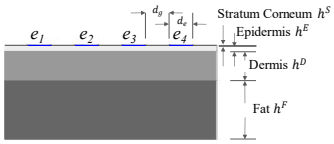
Once the $\gamma(\ln\tau)$ is retrieved, it provides a plot of $\gamma(\ln\tau)$ against τ. Hence, different relaxation mechanisms can be easily identified as a representation of frequency information where the conductivity change influences significantly or insignificantly on the impedance *Z*. Some of the frequency pairs are selected heuristically in order to calculate the impedance inputs α_ξ as shown in equations (4) to (7).

Generation of training data set by numerical simulation

Method and condition of numerical simulation

Numerical simulation studies are employed using finite element method (FEM) software to generate input for training data sets. The simulation of electric potential $\phi(\mathbf{r})$ inside a subdomain Ω is produced by placing a current across the surface skin in the boundary $\partial\Omega$ on each electrode transmitter with the injected current i [24].

Table 1: Parameters for training data set

Configuration parameter		**Measurement parameter**		
Injection pattern φ_s	**Electrode-length-to-skin-thickness ratio δ_b**	**Conductivity-changed layer ψ_p**	**Conductivity change $\Delta\sigma_q$ [%]**	**Frequency pair f_r^{lh} [kHz]**
I. Bipolar  II. Tetrapolar  	$D/H < 1, D/H = 1, D/H > 1$  Fixed electrode gap: $d_g = 1$ [mm] Variable electrode diameter: $d_e = \{1, 2, 3\}$[mm] Electrode length: $D = d_g + d_e$ Fixed each layer thickness: $h^S = 50$ [μm], $h^E = 0.45$ [mm], $h^D = 2.5$ [mm], $h^F = 5$ [mm] Fixed skin thickness: $H = h^S + h^E + h^D + h^F$	ψ_1 = Stratum Corneum only (S) ψ_2 = Epidermis (E) only ψ_3 = Dermis (D) only ψ_4 = Fat (F) only ψ_5 = S + E ψ_6 = E + D ψ_7 = D + F ψ_8 = S + E + D ψ_9 = E + D + F ψ_{10} = S + E + D + F	$\Delta\sigma_1 = -20$ $\Delta\sigma_2 = -17.5$ $\Delta\sigma_3 = -15$ $\Delta\sigma_4 = -12.5$ $\Delta\sigma_5 = -10$ $\Delta\sigma_6 = -7.5$ $\Delta\sigma_7 = -5$ $\Delta\sigma_8 = -2.5$ $\Delta\sigma_9 = 0$ $\Delta\sigma_{10} = 2.5$ $\Delta\sigma_{11} = 5$ $\Delta\sigma_{12} = 7.5$ $\Delta\sigma_{13} = 10$ $\Delta\sigma_{14} = 12.5$ $\Delta\sigma_{15} = 15$ $\Delta\sigma_{16} = 17.5$ $\Delta\sigma_{17} = 20$	$f_1^{lh} = 2$ & 10 $f_2^{lh} = 2$ & 35 $f_3^{lh} = 2$ & 100 $f_4^{lh} = 2$ & 225 $f_5^{lh} = 10$ & 35 $f_6^{lh} = 10$ & 100 $f_7^{lh} = 10$ & 225 $f_8^{lh} = 35$ & 100 $f_9^{lh} = 35$ & 225 $f_{10}^{lh} = 100$ & 225

i. $\Delta\sigma_9 = 0$ [%] is considered as standard.
ii. For each conductivity-changed layer, the other layer(s) are fixed with standard conductivity change value.
iii. Case number follow this rule: $\varphi_s_\delta_b_\psi_p_\Delta\sigma_q_f_r^{lh}$
(for example: I_$D/H < 1$_S_-20_2&10 which refers to injection pattern: φ_I = Bipolar_$\delta_1 = D/H < 1$, $\psi_1 = S$, $\Delta\sigma_1 = -20$, and $f_3^{lh} = 2$ & 100)
iv. Total case: $2(\varphi_s) \times 3(\delta_b) \times 10(\psi_p) \times 17(\Delta\sigma_q) \times 10(f_r^{lh}) = 10200$

$$\nabla \cdot \big(\sigma^*(\boldsymbol{r})\big)\nabla\phi(\boldsymbol{r}) = 0, \boldsymbol{r} \in \Omega \quad (17)$$

$$\phi(\boldsymbol{r}) + Z_c\sigma^*(\boldsymbol{r})\frac{\partial\phi(\boldsymbol{r})}{\partial \boldsymbol{n}} = U_l, \boldsymbol{r} \in e_l, l = \{1, \dots, L\} \quad (18)$$

$$\int_{\partial\Omega^{e_l}} \sigma^*(\mathbf{r})\frac{\partial\phi(\mathbf{r})}{\partial \mathbf{n}}\mathrm{d}S = I, \mathbf{r} \in \partial\Omega^{e_l} \quad (19)$$

$$\sigma^*(\mathbf{r})\frac{\partial\phi(\mathbf{r})}{\partial \mathbf{n}} = 0, \mathbf{r} \in \partial\Omega \backslash \bigcup_{l=1}^{L} e_l \quad (20)$$

where $\sigma^* := \sigma + 2\pi f\varepsilon \in \mathbb{C}\,[\mathrm{S\,m^{-1}}]$ is the nonhomogenous admittivity property of skin layer, σ and ε are the conductivity and absolute permittivity $[\mathrm{F\,m^{-1}}]$ respectively in Ω at the frequency f, $\phi(\mathbf{r}) \in \mathbb{C}\,[\mathrm{V}]$ is the electric potential distribution, and $\mathbf{r} := (x, y, z)$ is the coordinate system in subdomain Ω. **Table 1** shows the geometry of the skin layer model with BIS electrodes e_l. The contact impedance on each electrode is $Z_c = 50\ [\Omega]$. Meanwhile, the electrical properties of stratum corneum [25], epidermis, dermis [26], and fat [27] are adopted from several literatures. **Fig. 2** shows the comparison of conductivity $\sigma(\mathbf{r})$ and relative permittivity $\varepsilon_r(\mathbf{r})$ of each skin layer.

Input data for machine learning

1) Variation from standard conductivity change

Table 1 shows the conditions of the training data set generated by simulation. **Fig. 2** shows the variation of conductivity change $\Delta\sigma_q$ is defined from -20% to +20% from the conductivity σ value. The relative permittivity ε_r value is assumed constants for all the cases. The impedance inputs α_ξ are calculated from the impedance measurement at different frequency ranges $f = \{2, 10, 35, 100, 225\}$[kHz] selected through DRT from simulation and experiment data in the prior study. From this frequency range, the frequency pair f_r^{lh} in equations (8) to (11) are selected, as shown in **Table 1**.

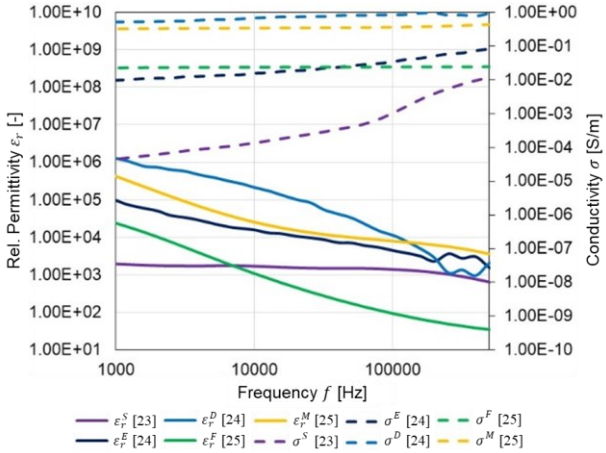


Fig. 2: Electrical properties of skin, fat, and muscle.

2) Electrode Length to Skin Thickness

The electrode length D, which combines the electrode diameter d_e and the gap between the electrodes d_g, plays an important role for the current penetration depth. In order to obtain a deeper electrical current penetration, D should be larger compared to the skin thickness H. As the electrical current penetration depth gets deeper, more tissue layers can be validated through BIS. Selecting the proper electrode-length-to-skin-thickness ratio δ_b is difficult because skin thickness is unknown during the BIS measurement. Consequently, the skin layer classification of conductivity change should consider the effect of *D/H*. More complicated variation of the electrode length is analyzed. However, the study is simplified by the three different conditions, i.e., $d_e = \{1, 2, 3\}\,[\mathrm{mm}]$. Also, H is constant as shown in **Table 1**, which includes the thickness of stratum corneum h^S, epidermis h^E, dermis h^D, and fat h^F layer. Thus, there are three different conditions of electrode-length-to-skin-thickness ratio δ_b: *D/H* < 1, *D/H* = 1, and *D/H* > 1.

3) Injection Patterns

In addition to the conductivity changes, evaluating different injection patterns is also considered in order to obtain the sensitivity of each injection pattern in the skin layer classification of conductivity change. **Table 1** shows a single bioimpedance measurement based on a colinear array that employs two injection patterns φ_s called bipolar and tetrapolar. Although, the tetrapolar configuration is commonly used as injection patterns to obtain the conductivity change information based on its capability to reduce an electrode-skin contact impedance. However, there is a trade-off between the electrode array area and the sensitivity to detect the conductivity change information according to its current pathway. Accordingly, other injection patterns are still adapted in some applications.

The bipolar configuration uses two electrodes, transmitting the current and receiving the voltage. The current density under the two electrodes is non-uniform, which results in non-linear impedance measurement to the variance of conductivity changes in the tissues. The impedance measurement of bipolar configuration is a superposition of three impedance sources: the wires impedance, the electrode-skin contact impedance, and the tissue impedance. The tetrapolar configuration uses four electrodes, two electrodes for transmitting the current and another two electrodes for receiving the voltage.

4) Labeling

In the supervised learning FNN, labeling refers to the process of assigning a label or category to input data based on the output of the neural network. In this case, each input data is assigned a case number representing the labeling for each injection pattern on the training data set. According to **Table 1**, the total case number equals 10200 data generated for the training data set. The classification into five groups (S, E, D, F, S+E) is based on the combination of possible conductivity changes in the skin layer. So, the only possible conductivity changes that occurred are S, E, D, F, S+E, and the adjacent layers. Because the objective is to distinguish specific data from particular layers, not layer combinations, considering layer combinations will lead to treating bulk skin, which differs from the goal. In addition, preliminary studies have shown that the conductivity change of the dermis layer hinders the conductivity change of other layers. As a result, layer combinations containing the dermis are treated the same as the class dermis. Considering all conditions, the arrangement of balanced datasets is maintained to achieve proper classification.

Feedforward Neural Network framework

The FNN in this paper was used as a supervised skin layer classification learner. Feedforward neural network (FNN) in this paper were implemented using a Matlab Machine Learning and Deep Learning Toolbox (Mathworks, Natick, MA, United States) on a laptop with CPU AMD Ryzen 7 PRO 4750U @1.7 GHz. K-fold = 5 is used to validate the accuracy. The accuracy *Acc* [%] is expressed as follows:

$$Acc = \frac{T_{\text{predict}}}{T_{\text{samples}}} \times 100 \qquad (21)$$

where, T_{predict} is the number of true predictions and T_{samples} is the number total samples used in the training data.

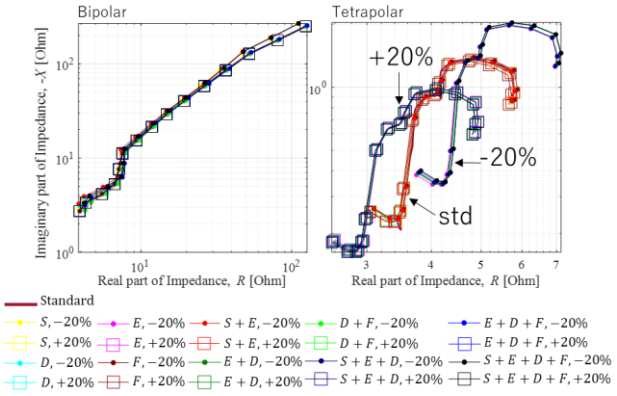


Fig. 3: Nyquist plot based on numerical simulation of φ_s in the $\Delta\sigma$ and *D/H* < 1 in all frequency range.

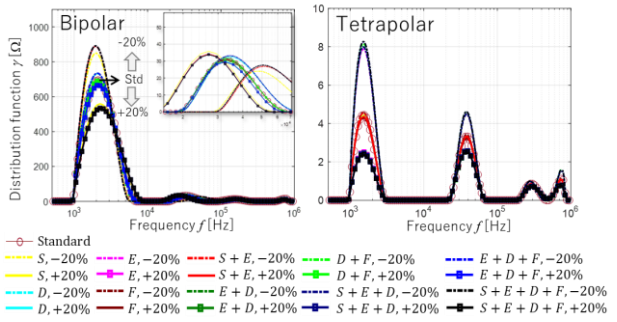


Fig. 4: DRT results based on simulation of φ_s in the case of *D/H* < 1 in all frequency range.

Table 2: Matrix profile of α_ξ

Matrix Profile	Number of input features α_ξ	Details
One matrix	4	$\acute{Z}, \acute{\theta}, \acute{R}, \acute{X}$
Two matrices	6	$\acute{Z}+\acute{\theta}, \acute{Z}+\acute{R}, \acute{Z}+\acute{X}, \acute{\theta}+\acute{R}, \acute{\theta}+\acute{X}, \acute{R}+\acute{X}$
Three matrices	3	$\acute{Z}+\acute{\theta}+\acute{R}, \acute{Z}+\acute{\theta}+\acute{X}, \acute{\theta}+\acute{R}+\acute{X}$
Four matrices	1	$\acute{Z}+\acute{\theta}+\acute{R}+\acute{X}$

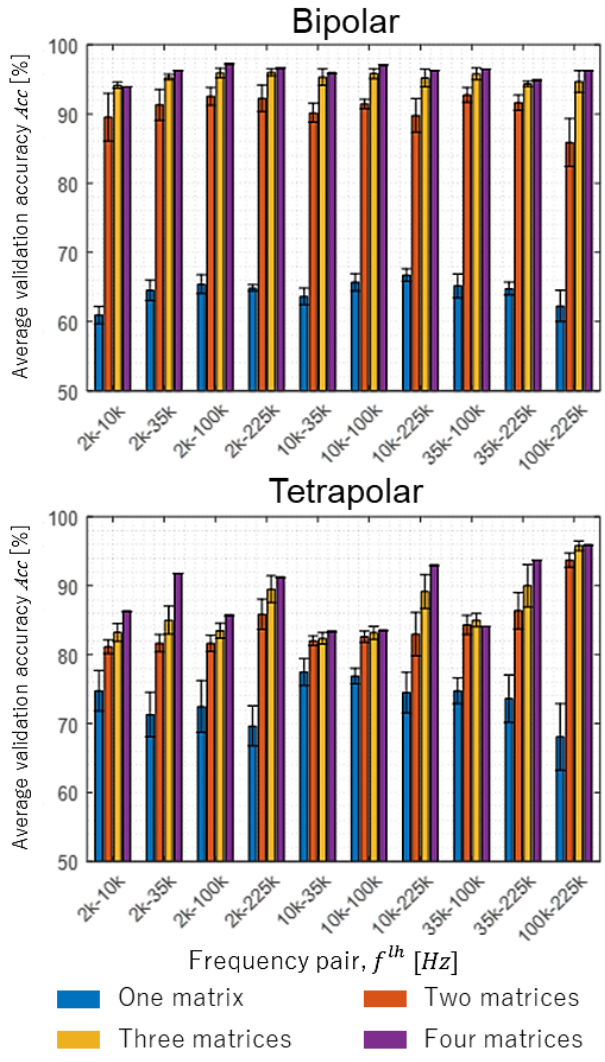


Fig. 5: The comparison of FNN results related to feature extraction of α_ξ effect on bipolar and tetrapolar.

Training data set by numerical simulation

Impedance by numerical simulation

Fig. 3 shows the comparison of the Nyquist plot from the impedance measurement of two φ_s in the case of all ψ_p with $\Delta\sigma_q = \{-20, 0(\text{standard}), +20\}[\%]$ where D/H < 1 in all frequencies. The impedance spectrums in the Nyquist plot change slightly among the different conductivity change variations. The tendency of the impedance spectrum from the bipolar set-up is similar to the behavior with a Warburg impedance. Meanwhile, in the case of the tetrapolar set-up, the impedance spectrum has some electrical behaviors, which are a charge transfer, dielectric interphase, conductive part, and diffusion part. Nevertheless, the conductivity change is difficult to classify from these data representations.

Distribution of relaxation times

The slight changes due to different conductivity shown in the Nyquist plot from simulation is well translated by DRT as shown in **Fig. 4**, which displays multiple local maxima towards higher gamma values as the conductivity increases toward different skin layer acquired from two φ_s in the case of all ψ_p with $\Delta\sigma_q = \{-20, 0(\text{standard}), +20\}[\%]$ where D/H < 1 in all frequencies. By inspection, the DRT serves as an indicator given the retrieved relaxation times of each skin layer. The local maxima observed begin and end by local minimum. Hence, this local minimum between the local maxima is important as indication of the frequency range applied to a skin layer. This observation forms the basis for determining the frequency pairs of each skin layer where changes in conductivity have significant or insignificant effects.

Feature extraction based on impedance inputs α_ξ

As part of pre-processing data for FNN, feature extraction is performed to select only the features that would contribute most to the quality of data features that will be highly correlated with the output. The introduction of four impedance inputs with a wide range of frequencies leads to feature extraction with several options called one matrix, two matrices, three matrices, and four matrices profile, as shown in **Table 2**.

Feature extraction will evaluate the matrices by comparison of average validation accuracy results. **Fig. 5** shows the comparison of FNN average accuracy *Acc* regarding to the matrix of impedance inputs. The figure illustrates that as the number of inputs increases, the accuracy increases for both bipolar and tetrapolar injection patterns. This finding suggests a positive correlation between

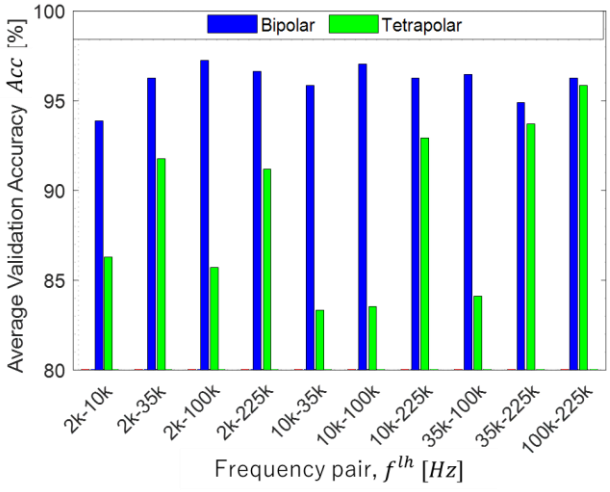
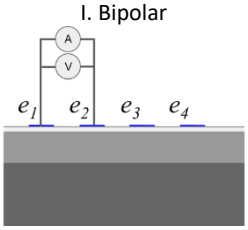
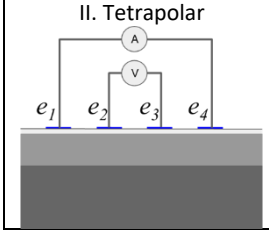
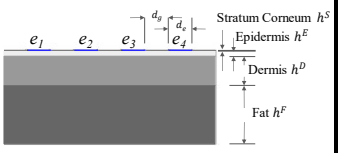


Fig. 6: The comparison of FNN results related to feature extraction of α_ξ effect on bipolar and tetrapolar using four matrices profile.

Table 3: Experimental conditions

Configuration parameter		Measurement parameter		
Injection pattern φ_s	**Electrode length ratio to skin thickness δ_b**	**Conductivity-changed layer y_p**	**Concentration c_{NaCl} [mM]**	**Frequency pair f_r^{lh} [kHz]**
I. Bipolar  II. Tetrapolar 	$D/H < 1, D/H = 1, D/H > 1$ 	Dermis (D) only	$c_1 = 15$ $c_2 = 20;$ $c_3 = 25;$ $c_4 = 30;$ $c_5 = 35;$	$f_1^{lh} = 2 \& 10;$ $f_2^{lh} = 2 \& 35;$ $f_3^{lh} = 2 \& 100;$ $f_4^{lh} = 2 \& 225;$ $f_5^{lh} = 10 \& 35;$ $f_6^{lh} = 10 \& 100;$ $f_7^{lh} = 10 \& 225;$ $f_8^{lh} = 35 \& 100;$ $f_9^{lh} = 35 \& 225;$ $f_{10}^{lh} = 100 \& 225$

the number of inputs and accuracy. The four matrices profile shows the highest accuracy in all selected frequency pairs, meaning the selected features on the four matrices profile are relevant to achieve better accuracy on the validation sets, as shown in **Fig. 6**.

Experiments

Experimental setup

Fig. 7 shows the experimental setup composed of a co-planar sensor with multiple electrodes, an impedance analyzer (IM3570, Hioki EE Corporation, Tokyo, Japan) as a data acquisition system, a switching, and a PC for command and post-processing. The electrodes are manufactured on a printed circuit board and made of stainless steel with a diameter of 1 mm, a height of 1 mm, and distance between both electrodes is 1 mm.

In bipolar mode, one electrode serves as the current injector and high potential electrode in a two-wire measuring system, while the other electrode serves as the ground and low potential electrode. In tetrapolar mode, e_1 acts as the current injector, e_2 serves as the high potential electrode, the low potential electrode is e_3, and the ground electrode is performed by e_4. The ground electrode receives current from the current injector electrode as it passes through the measuring object. The high potential and low potential electrodes simultaneously measure the voltage produced by the current flow.

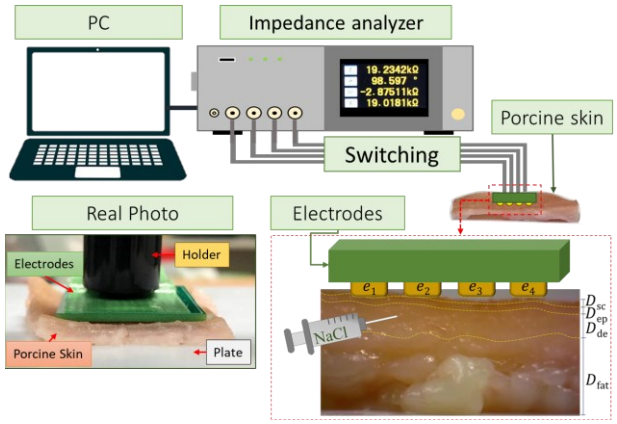


Fig. 7: Experimental setup conditions with porcine skin.

Experimental method and conditions

Porcine skin was used as the measurement object because of its comparable mechanical and electrical characteristics to human skin. Several studies have shown that porcine skin is similar to human skin in general structures [28], thickness [29], lipid composition [30], and dielectric properties [31]. While human skin varies from person to person, porcine skin remains a valuable model for human skin studies.

The porcine skin still bound together the muscle and fat. The sample must first be adjusted to the proper temperature (about 35 °C), after which extra layers of fat and muscle must be removed, leaving only the stratum corneum, epidermis, and dermis, along with one layer of fat and one layer of muscle, to maintain accurate measurements throughout the experiment.

In order to validate the proposed method, an experiment with porcine skin is used by creating variation in conductivity by injecting saline water into the dermis layer. Our study divided a large-sized pig skin into five samples based on the NaCl concentration levels. For both the bipolar and tetrapolar injection patterns, each sample underwent three injections at different locations within the dermis layer. Subsequently, we performed three repeated measurements at each location. Therefore, in summary, each sample was subjected to nine measurements. The average of these measurements was then used as the input for the validation dataset in the FNN model, specifically for the dermis (D) layer, as specified in **Table 3.** Saline water, with a concentration of $c_{NaCl} = 25$ [mM], is considered the standard value. This experiment`s conditions are to mimic the conductivity change at the dermis layer artificially [32].

The impedance measurement method is bipolar and tetrapolar with $i = 1$ [mA] and frequency pair f_r^{lh} as used in the simulation. The electrode-length-to-skin-thickness ratios are *D/H* < 1, *D/H* = 1, and *D/H* > 1.

Ethical approval

The research related to animals use has been complied with all the relevant national regulations and institutional policies for the care and use of animals.

Results and discussion

Frequency pair f_r^{lh} selection by DRT

Based on the results from DRT, **Fig. 8** and **Fig. 9** show the distribution function γ in all frequencies under various concentrations and all electrode-length-to-skin-thickness ratios for bipolar and tetrapolar mode, respectively, for the experimental studies. Different distribution function values of several local maximums also represent different conductivity change values from different concentrations, which means the system is indistinguishable and requires further investigation. Several local maximums are observed in both figures representing optimum frequencies at which the system exhibits maximum sensitivity or the most informative response. Hence, it gives a range of frequencies of interest that could be the location to extract the informative response of the system, which can be used for further investigation, in this particular case, for classification.

At high-frequency ranges, information about the stratum corneum known to have high resistance requires additional investigation [25]. The distribution function in the medium frequency regions is relatively low, requiring further experiments and analysis regarding the epidermis layer. Finally, the local maxima are due to dermis layer effect at low-frequency ranges since the increased injected saline water concentration is related to the decreased local maxima [17]. The distribution of relaxation time in simulation and experiment shows a similar trend. Thus, the heuristic selection of frequency pair shown in **Table 3** is acceptable.

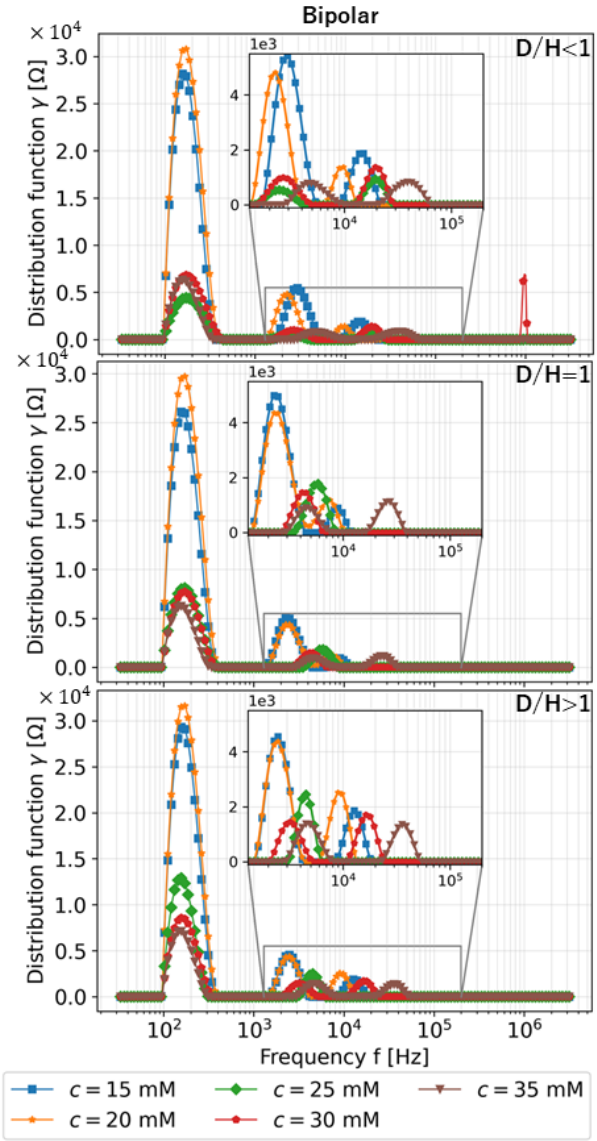


Fig. 8: DRT results based on experiment with φ_s = Bipolar in all frequencies.

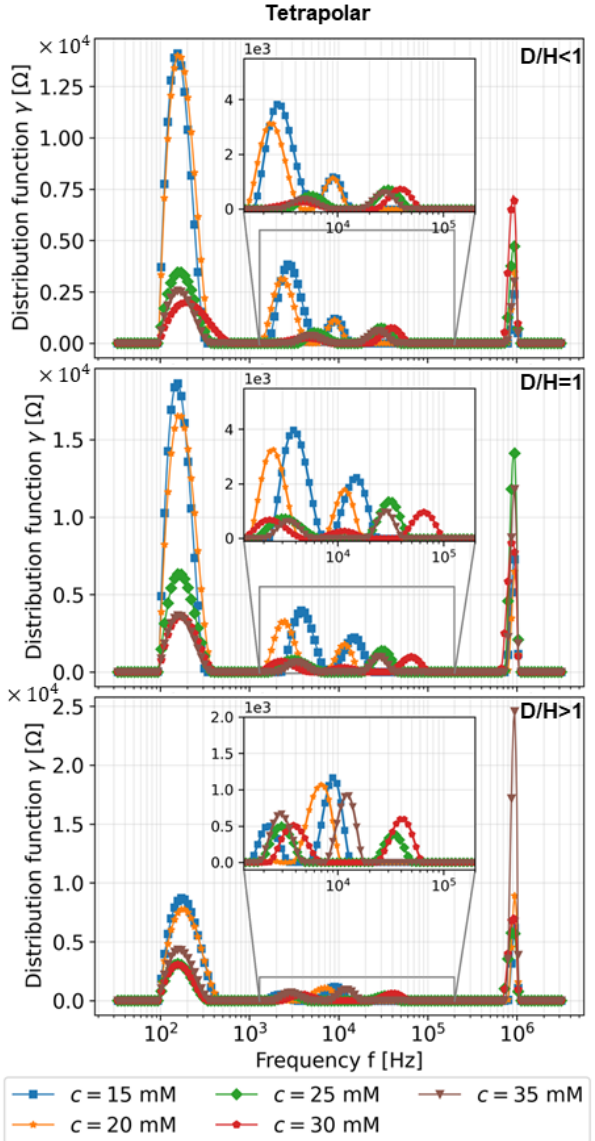


Fig. 9: DRT results based on experiment with φ_s = Tetrapolar in all frequencies.

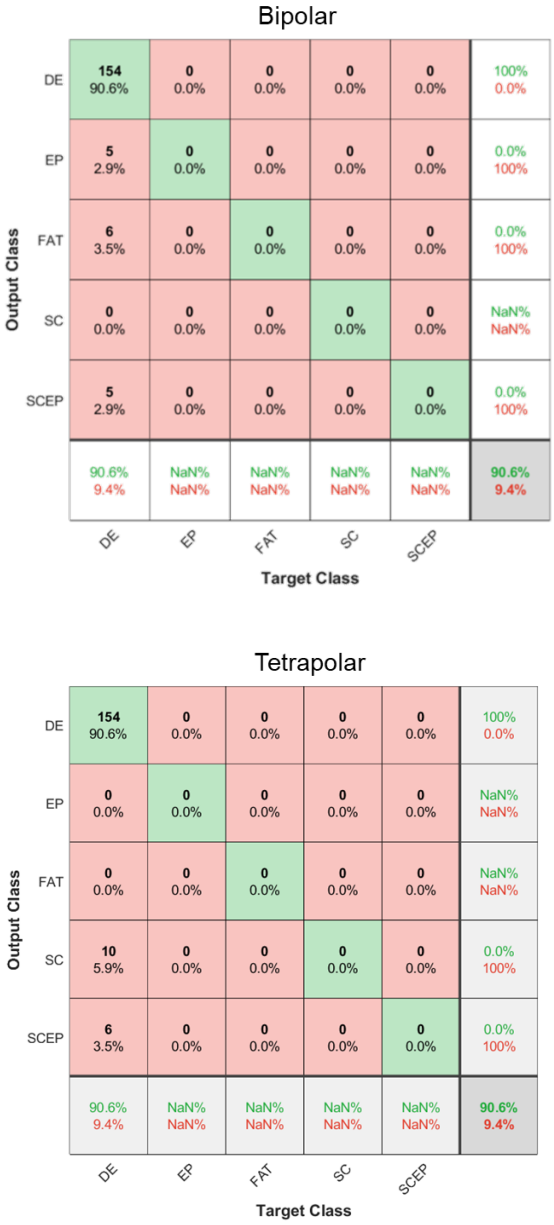


Fig. 10: The confusion matrix shows the highest validation accuracy of experiments of porcine skin with FNN and four impedance inputs α_ξ.

Table 4: Comparison of FNN accuracy *Acc* in terms of variation of frequency pair selection from experiment results.

Frequency pair f_r^{lh} [kHz]	**Bipolar *Acc* [%]**	**Tetrapolar *Acc* [%]**
$f_1^{lh} = 2 \,\&\, 10$	44.1	1.2
$f_2^{lh} = 2 \,\&\, 35$	80.6	17.6
$f_3^{lh} = 2 \,\&\, 100$	56.5	16.5
$f_4^{lh} = 2 \,\&\, 225$	40.6	10.0
$f_5^{lh} = 10 \,\&\, 35$	88.8	90.0
$f_6^{lh} = 10 \,\&\, 100$	90.6	84.1
$f_7^{lh} = 10 \,\&\, 225$	61.2	32.4
$f_8^{lh} = 35 \,\&\, 100$	60.6	90.6
$f_9^{lh} = 35 \,\&\, 225$	55.3	25.3
$f_{10}^{lh} = 100 \,\&\, 225$	68.2	23.5

Skin layer classification

The confusion matrix is a useful tool for evaluating the performance of a classification model. In our studies, the FNN for bipolar mode at f_6^{lh} achieved a high classification accuracy of 90.6% for the dermis layer (DE), which is promising. However, there were still some misclassifications, with 2.9% classified as epidermis (EP), 3.5% as fat (FAT), and 2.9% as stratum corneum and epidermis layers (SCEP). For tetrapolar mode at f_8^{lh}, the result showed that 90.6% of DE was classified correctly, while EP and FAT were classified at 0.0%, stratum corneum (SC) at 5.9%, and the SCEP at 3.5%, as shown in **Fig. 10**. The 0.0% classification in the confusion matrix does not indicate an error or confusion of DE for SC in bipolar or EP and FAT in tetrapolar injection patterns. Instead, it signifies that there were no instances of misclassification between these specific classes. Furthermore, the amount of data used in the analysis is sufficient for the purpose of this study. Also, it is important to note that the experimental conditions involved only the DE class for the model. While the overall accuracy is accountable, the misclassifications suggest room for improvement in the model.

One potential reason for the misclassifications could be the similarity between the dermis and epidermis layers in terms of their electrical properties [26]. Future studies could consider incorporating additional features [33] or imaging techniques [34], highlighting the importance of continuing to refine the model and improving the accuracy of the classification for these layers. Overall, the confusion matrix results demonstrate the potential of the FNN in accurately classifying skin layers but also highlight the need for further optimization and refinement of the model.

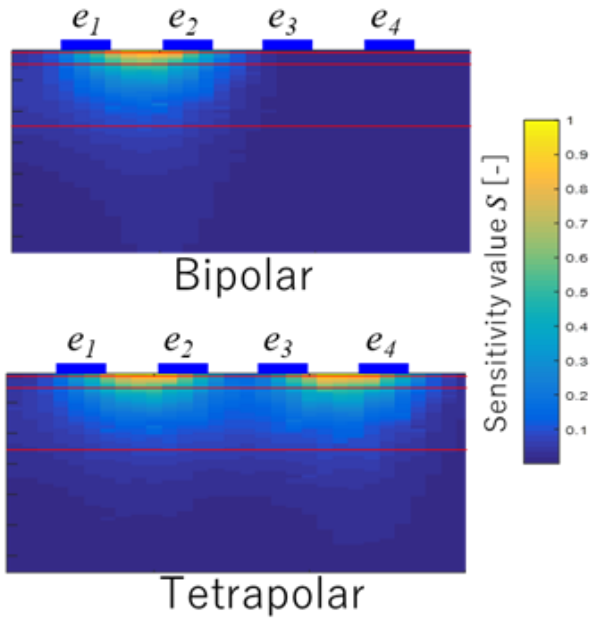


Fig. 11: Comparison of sensitivity map distribution: bipolar and tetrapolar.

Table 4 compares the FNN accuracy *Acc* between bipolar and tetrapolar injection patterns in each frequency pair variation. It shows that bipolar mode at f_6^{lh} achieved the highest accuracy, *Acc* 90.6% and tetrapolar mode at f_8^{lh} achieved the same accuracy. The study focused primarily on evaluating the classification performance and the influence of different injection patterns. It did not explicitly assess the effect of systematic error during the measurement. However, it is important to note that inherent systematic errors exist in the experimental results. Frequency pair is one of the ways to minimize this effect because systematic error due to stray capacitance or contact impedance is also frequency dependent. The discrepancy in performance between bipolar and tetrapolar injection patterns can be attributed to the difference in current pathway lengths. The variation in current pathway length directly affects the sensitivity of the measurement, as shown in **Fig. 11**. Therefore, the performances observed in **Table 4** result from these differences in current pathway length.

Reliability of FNN

The study found that the FNN demonstrated promising results as a tool for skin layer classification, along with other bioelectrical impedance spectroscopy post-processing approaches.

Two injection patterns were employed to train the FNN, and while they performed differently, both had high accuracy. In order to validate these discrepancies, the sensitivity matrix map was used, which showed the effective area that passed by the electrical current distribution during the impedance measurement, as shown in **Fig. 11**. Although the sensitivity matrix map could differ from actual skin layer circumstances, it gave insight into the penetration depth of the electrical current under ideal conditions [35].

Real scenarios often involve an unknown skin thickness, making it difficult to evaluate the penetration depth of the electrical current by adjusting the electrode length. The study tested three different electrode-to-skin thickness ratios (D/H): D/H < 1, D/H = 1, and D/H > 1, corresponding to -10% to +50% of the skin thickness range. Under these conditions, results showed that the FNN had high accuracy rates in classifying skin layers in simulations and experiments. However, it could be challenging to obtain accurate results with electrode lengths similar to those of common biopotential electrodes like ECG (5 mm) or electro-myography (10 mm). Further studies are necessary to investigate this issue.

Reliability of training data features

The impedance inputs α_{ξ}, proposed in this study, shows the reliability of features extraction to classify the conductivity change in the BIS measurement for skin layer classification. Using the impedance inputs α_{ξ} in the FNN training reduces the number of training data significantly.

The conductivity change of skin layer affects all the impedance measurement parameters, which are impedance, phase angle, resistance, and reactance. By evaluating the results of **Fig. 4**, the impedance inputs α_{ξ} in equations (4) to (7) are representations of a ratio metric form that amplifies the presence of conductivity change. As a result, the impedance inputs α_{ξ} reduce the ill-posed problem of impedance measurement for skin layer classification of conductivity change.

In the experiment, measurement noise and systematic error inherently appear and are difficult to consider in the simulation. Nonetheless, the proposed method was confirmed by the experiment with skin because the data featuring based on impedance inputs α_{ξ} at the selected frequency pair successfully eliminates the conductivity change that are not from the skin layer.

Conclusions

In this study, the three objectives have been proposed for skin layer classification of conductivity change in skin layer, which are (1) to predict the validation accuracy of dermis classification by implementing feedforward neural network (FNN), (2) to minimize the unnecessary training data of FNN using four impedance inputs α_{ξ}, which are the magnitude input $\alpha_{|\boldsymbol{Z}|}$, phase angle input α_{θ}, resistance input α_{R}, and reactance input α_{X}, and (3) to select the frequency pair f_r^{lh}.

From the simulation and experimental validation, some concluding remarks are as follows:

1) The trained FNN shows the highest accuracy *Acc* for bipolar and tetrapolar are 97.25% at f_2^{lh} and 95.88% at f_{10}^{lh}, respectively, in the case of simulation. The experiment for bipolar has the highest accuracy, *Acc* = 90.6% at f_6^{lh} and tetrapolar has *Acc* = 90.6% at f_8^{lh}.
2) The impedance inputs α_{ξ} reduce the number of training data but has reliable data featuring FNN training by showing a high accuracy. All four proposed impedance inputs α_{ξ} should be used to obtain a highest *Acc* for all injection patterns.
3) The frequency pair selection is satisfactory as bipolar mode has the highest validation accuracy *Acc* at f_6^{lh}, while tetrapolar mode has the highest accuracy *Acc* at f_8^{lh}.

Conflict of interest

Authors state no conflict of interest.

References

1. Nicander I, Ollmar S. Electrical Bioimpedance Related to Structural Differences and Reactions in Skin and Oral Mucosa. Ann New York Acad Sci. 1999;873(1):221-6. https://doi.org/10.1111/j.1749-6632.1999.tb09470.x

2. Abe Y, Nishizawa M. Electrical aspects of skin as a pathway to engineering skin devices. APL Bioeng. 2021;5(4). https://doi.org/10.1063/5.0064529
3. Rifai IN, Baidillah MR, Wicaksono R, Akita S, Takei M. Quantification of dermis sodium concentration in skin layers by power spectral density drop of square-wave electrical impedance spectroscopy (PSDd-sEIS). Meas Sci Technol. 2023;34(7):74006. https://doi.org/10.1088/1361-6501/acc752
4. Uchiyama T, Ishigame S, Niitsuma J, Aikawa Y, Ohta Y. Multi-frequency bioelectrical impedance analysis of skin rubor with two-electrode technique. J Tissue Viability. 2008;17(4):110-4. https://doi.org/10.1016/j.jtv.2008.01.002
5. Braun RP, Mangana J, Goldinger S, French L, Dummer R, Marghoob AA. Electrical impedance spectroscopy in skin cancer diagnosis. Dermatol Clin. 2017;35(4):489-93. https://doi.org/10.1016/j.det.2017.06.009
6. Nyström J, Lindholm-Sethson B, Stenberg L, Ollmar S, Eriksson JW, Geladi P. Combined near-infrared spectroscopy and multifrequency bio-impedance investigation of skin alterations in diabetes patients based on multivariate analyses. Med Biol Eng Comput. 2003;41(3):324-9. https://doi.org/10.1007/BF02348438
7. Nicander I, Ollmar S, Rozell BL, Eek A, Emtestam L. Electrical impedance measured to five skin depths in mild irritant dermatitis induced by sodium lauryl sulphate. Br J Dermatol. 1995;132(5):718-24. https://doi.org/10.1111/j.1365-2133.1995.tb00716.x
8. Emtestam L, Ollmar S. Electrical impedance index in human skin: measurements after occlusion, in 5 anatomical regions and in mi Id irritant contact dermatitis. Contact Dermatitis. 1993;28(2):104-8. https://doi.org/10.1111/j.1600-0536.1993.tb03352.x
9. Martinsen ØG, Grimnes S, Haug E. Measuring depth depends on frequency in electrical skin impedance measurements. Ski Res Technol. 1999;5(3):179-81. https://doi.org/10.1111/j.1600-0846.1999.tb00128.x
10. Arpaia P, Cesaro U, Moccaldi N. A bioimpedance meter to measure drug in transdermal delivery. IEEE Trans Instrum Meas. 2018;67(10):2324-31. https://doi.org/10.1109/TIM.2018.2817399
11. Andreasen N, Crandall H, Brimhall O, Miller B, Perez-Tamayo J, Martinsen OG, et al. Skin Electrical Resistance as a Diagnostic and Therapeutic Biomarker of Breast Cancer Measuring Lymphatic Regions. IEEE Access. 2021;9:152322-32. https://doi.org/10.1109/ACCESS.2021.3123569
12. Gessert N, Bengs M, Schlaefer A. Melanoma detection with electrical impedance spectroscopy and dermoscopy using joint deep learning models. In: Medical Imaging 2020: Computer-Aided Diagnosis. SPIE; 2020. p. 265-71. https://doi.org/10.1117/12.2548974
13. Kawahara J, Daneshvar S, Argenziano G, Hamarneh G. Seven-point checklist and skin lesion classification using multitask multimodal neural nets. IEEE J Biomed Heal informatics. 2018;23(2):538-46. https://doi.org/10.1109/JBHI.2018.2824327
14. Barragán-Moreno A, Schaltz E, Gismero A, Stroe DI. Capacity State-of-Health Estimation of Electric Vehicle Batteries Using Machine Learning and Impedance Measurements. Electron. 2022;11(9). https://doi.org/10.3390/electronics11091414
15. Van Haeverbeke M, Stock M, De Baets B. Equivalent Electrical Circuits and Their Use Across Electrochemical Impedance Spectroscopy Application Domains. IEEE Access. 2022;10:51363-51379. https://doi.org/10.1109/ACCESS.2022.3174067
16. Wan TH, Saccoccio M, Chen C, Ciucci F. Influence of the Discretization Methods on the Distribution of Relaxation Times Deconvolution: Implementing Radial Basis Functions with DRTtools. Vol. 184, Electrochimica Acta. 2015;184:483-99. https://doi.org/10.1016/j.electacta.2015.09.097
17. Ramirez-Chavarria RG, Sanchez-Perez C, Romero-Ornelas L, Ramon-Gallegos E. Time-Constant-Domain Spectroscopy: An Impedance-Based Method for Sensing Biological Cells in Suspension. IEEE Sens J. 2021;21(1):185-92. https://doi.org/10.1109/JSEN.2020.3014569
18. Ollmar S. Methods of information extraction from impedance spectra of biological tissue, in particular skin and oral mucosa-a critical review and suggestions for the future. Bioelectrochemistry Bioenerg. 1998;45(2):157-60. https://doi.org/10.1016/S0302-4598(98)00082-8
19. Oz A, Hershkovitz S, Belman N, Tal-Gutelmacher E, Tsur Y. Analysis of impedance spectroscopy of aqueous supercapacitors by evolutionary programming: finding DFRT from complex capacitance. Solid State Ionics. 2016;288:311-4. https://doi.org/10.1016/j.ssi.2015.11.008
20. Tuncer E, Macdonald JR. Comparison of methods for estimating continuous distributions of relaxation times. J Appl Phys. 2006;99(7):74106. https://doi.org/10.1063/1.2188053
21. Schichlein H, Müller AC, Voigts M, Krügel A, Ivers-Tiffée E. Deconvolution of electrochemical impedance spectra for the identification of electrode reaction mechanisms in solid oxide fuel cells. J Appl Electrochem. 2002;32(8):875-82. https://doi.org/10.1023/A:1020599525160
22. Sonn V, Leonide A, Ivers-Tiffée E. Combined deconvolution and CNLS fitting approach applied on the impedance response of technical Ni∕8YSZ cermet electrodes. J Electrochem Soc. 2008;155(7):B675. https://doi.org/10.1149/1.2908860
23. Dierickx S, Weber A, Ivers-Tiffée E. How the distribution of relaxation times enhances complex equivalent circuit models for fuel cells. Electrochim Acta. 2020;355:136764. https://doi.org/10.1016/j.electacta.2020.136764
24. Somersalo E, Cheney M, Isaacson D. Existence and uniqueness for electrode models for electric current computed tomography. SIAM J Appl Math. 1992;52(4):1023-40. https://doi.org/10.1137/0152060
25. Yamamoto T, Yamamoto Y. Electrical properties of the epidermal stratum corneum. Med Biol Eng. 1976;14(2):151-8. https://doi.org/10.1007/BF02478741
26. Tsai B, Xue H, Birgersson E, Ollmar S, Birgersson U. Dielectrical properties of living epidermis and dermis in the frequency range from 1 kHz to 1 MHz. J Electr Bioimpedance. 2019;10(1):14-23. https://doi.org/10.2478/joeb-2019-0003
27. Andreuccetti D, Fossi R, Petrucci C. An Internet resource for the calculation of the dielectric properties of body tissues in the frequency range 10 Hz-100 GHz. IFAC-CNR, Florence (Italy). IFAC-CNR; 1997.
28. Summerfield A, Meurens F, Ricklin ME. The immunology of the porcine skin and its value as a model for human skin. Mol

Immunol. 2015;66(1):14-21. https://doi.org/10.1016/j.molimm.2014.10.023

29. Meyer W, Schwarz R, Neurand K. The skin of domestic mammals as a model for the human skin, with special reference to the domestic pig1. In: Skin-drug application and evaluation of environmental hazards. Karger Publishers; 1978. p. 39-52. https://doi.org/10.1159/000401274
30. Debeer S, Le Luduec JB, Kaiserlian D, Laurent P, Nicolas JF, Dubois B, et al. Comparative histology and immunohistochemistry of porcine versus human skin. Eur J Dermatology. 2013;23(4):456-66. https://doi.org/10.1684/ejd.2013.2060
31. Karacolak T, Cooper R, Unlu ES, Topsakal E. Dielectric properties of porcine skin tissue and in vivo testing of implantable antennas using pigs as model animals. IEEE Antennas Wirel Propag Lett. 2012;11:1686-9. https://doi.org/10.1109/LAWP.2013.2241722
32. Wake K, Sasaki K, Watanabe S. Conductivities of epidermis, dermis, and subcutaneous tissue at intermediate frequencies. Phys Med Biol. 2016;61(12):4376-89. https://doi.org/10.1088/0031-9155/61/12/4376
33. Pessoa D, Rocha BM, Cheimariotis GA, Haris K, Strodthoff C, Kaimakamis E, et al. Classification of Electrical Impedance Tomography Data Using Machine Learning. In: 2021 43rd Annual International Conference of the IEEE Engineering in Medicine & Biology Society (EMBC). 2021. p. 349-53. https://doi.org/10.1109/EMBC46164.2021.9629961
34. Rifai IN, Baidillah MR, Wicaksono R, Akita S, Takei M. Sodium concentration imaging in dermis layer by square-wave open electrical impedance tomography (SW-oEIT) with spatial voltage thresholding (SVT). Biomed Phys Eng Express. 2023;9(4):45013. https://doi.org/10.1088/2057-1976/acd4c6
35. Kim MS, Cho Y, Seo ST, Son CS, Park HJ, Kim YN. A new method for non-invasive measurement of skin in the low frequency range. Healthc Inform Res. 2010;16(3):143-8. https://doi.org/10.4258/hir.2010.16.3.143
36. Ramos A, Bertemes-Filho P. Numerical sensitivity modeling for the detection of skin tumors by using tetrapolar probe. Electromagn Biol Med. 2011;30(4):235-45. https://doi.org/10.3109/15368378.2011.589555
37. Ferreira DM, Silva CS, Souza MN. Electrical impedance model for evaluation of skin irritation in rabbits and humans. Ski Res Technol. 2007;13(3):259-67. https://doi.org/10.1111/j.1600-0846.2007.00217.x
38. Luo X, Zhou Y, Smart T, Grossman D, Sanchez B. Electrical Characterization of Basal Cell Carcinoma Using a Handheld Electrical Impedance Dermography Device. JID Innov. 2022;2(1):100075. https://doi.org/10.1016/j.xjidi.2021.100075
39. Sarac E, Meiwes A, Eigentler TK, Forchhammer S, Kofler L, Häfner HM, et al. Diagnostic accuracy of electrical impedance spectroscopy in non-melanoma skin cancer. Acta Derm Venereol. 2020;100(18):1-5. https://doi.org/10.2340/00015555-3689

Appendix A

Table 5: Comparison studies of skin condition detection using only BIS or combined with machine learning algorithm.

No	Author	Skin Condition	Machine Learning Algorithm & Data Features	Frequency Pair Selection & Reason	Injection Patterns
1	Stig Ollmar [18]	Oral mucosa	*NA* & $\acute{Z}$, $\acute{\theta}$, $\acute{R}$, and $\acute{X}$	20 [kHz] & 50 [kHz]: *NA*	Bipolar
2	Nicander et al. [7]	Irritant dermatitis	*NA* & $\acute{Z}$	20 [kHz] & 1 [MHz]: *NA*	Bipolar
3	Ramos & Bertemes-Filho [36]	Skin cancer	*NA* & Electrical equivalent circuit	100 [Hz] – 1 [MHz]: To analyze the tetrapolar probe's sensitivities' frequency response. It was discovered that frequency has little effect on sensitivity.	Tetrapolar
4	Ferreira et al. [37]	Skin irritation	*NA* & Resistance ratio from two depth locations	20 [kHz] & 50 [kHz]: The ratio of total skin impedance obtained at low (20 [kHz]) and high frequencies (500 [kHz]) is the basis of the irritation indices.	Bipolar
5	Gessert et al. [12]	Skin melanoma	CNN and SVM & $\acute{Z}$ and Images	1 [kHz] – 2.5 [MHz]: Following the device's frequency range.	Bipolar
6	Luo et al. [38]	Skin cancer	*NA* & Transversal and longitudinal of relative permittivity and conductivity	8 – 256 [kHz]: For measurements of lesional and normal skin, intraclass correlation coefficient (ICC) conductivity values were low at 8 and 16 [kHz]. In contrast, relative permittivity ICC results displayed excellent repeatability at 16 [kHz].	Tetrapolar
7	Sarac et al. [39]	Skin cancer	*NA* & EIS Score	1 [kHz] – 2.5 [MHz]: The extracellular environment affects resistance to low frequencies, whereas both the intracellular and extracellular environments influence readings at higher frequencies.	Bipolar
8	This study	Skin layer classification	FNN & $\alpha_{\|Z\|}$, α_{θ}, α_{R}, and α_{X}	f_r^{lh} are selected based on DRT results.	Bipolar, Tetrapolar

Abbreviations: CNN, convolutional neural network; SVM, support vector machine; FNN. feedforward neural network.